

Tailoring the optical and magnetic properties of La-BaM hexaferrites by Ni substitution

Hafiz T. Ali, M. Ramzan, M Imran Arshad, Nicola A. Morley, M. Hassan Abbas, Mohammad Yusuf, Atta Ur Rehman, Khalid Mahmood, Adnan Ali, Nasir Amin, and M. Ajaz-un-Nabi

Citation: Chin. Phys. B, 2022, 31 (**2**): 027502. DOI: 10.1088/1674-1056/ac1412

Journal homepage: http://cpb.iphy.ac.cn; http://iopscience.iop.org/cpb

What follows is a list of articles you may be interested in

Optimized growth of compensated ferrimagnetic insulator $Gd_3Fe_5O_{12}$ with a perpendicular magnetic anisotropy

Heng-An Zhou(周恒安), Li Cai(蔡立), Teng Xu(许腾), Yonggang Zhao(赵永刚), and Wanjun Jiang(江万军)

Chin. Phys. B, 2021, 30 (**9**): 097503. DOI: 10.1088/1674-1056/ac0db0

Magnetic dynamics of two-dimensional itinerant ferromagnet Fe_3GeTe_2

Lijun Ni(倪丽君), Zhendong Chen(陈振东), Wei Li(李威), Xianyang Lu(陆显扬), Yu Yan(严羽), Longlong Zhang(张龙龙), Chunjie Yan(晏春杰), Yang Chen(陈阳), Yaoyu Gu(顾耀玉), Yao Li(黎遥), Rong Zhang(张荣), Ya Zhai(翟亚), Ronghua Liu(刘荣华), Yi Yang(杨燚), and Yongbing Xu(徐永兵)

Chin. Phys. B, 2021, 30 (**9**): 097501. DOI: 10.1088/1674-1056/ac0e25

Effective model for rare-earth Kitaev materials and its classical Monte Carlo simulation

Mengjie Sun(孙梦杰), Huihang Lin(林慧航), Zheng Zhang(张政), Yanzhen Cai(蔡焱桢), Wei Ren(任玮), Jing Kang(康靖), Jianting Ji(籍建葶), Feng Jin(金峰), Xiaoqun Wang(王孝群), Rong Yu(俞榕), Qingming Zhang(张清明), and Zhengxin Liu(刘正鑫)

Chin. Phys. B, 2021, 30 (**8**): 087503. DOI: 10.1088/1674-1056/ac0a5d

Microstructure and magnetocaloric properties in melt-spun and high-pressure hydrogenated $La_{0.5}Pr_{0.5}Fe_{11.4}Si_{1.6}$ ribbons

Qian Liu(刘倩), Min Tong(佟敏), Xin-Guo Zhao(赵新国), Nai-Kun Sun(孙乃坤), Xiao-Fei Xiao(肖小飞), Jie Guo(郭杰), Wei Liu(刘伟), and Zhi-Dong Zhang(张志东)

Chin. Phys. B, 2021, 30 (**8**): 087502. DOI: 10.1088/1674-1056/abea91

Magnetic properties and resistivity of a 2:17-type SmCo magnet doped with ZrO_2

Qi-Qi Yang(杨棋棋), Zhuang Liu(刘壮), Chao-Yue Zhang(张超越), Hai-Chen Wu(吴海辰), Xiao-Lei Gao(高晓磊), Yi-Long Ma(马毅龙), Ren-Jie Chen(陈仁杰), and A-Ru Yan(闫阿儒)

Chin. Phys. B, 2021, 30 (**7**): 077504. DOI: 10.1088/1674-1056/abf7a9

Tailoring the optical and magnetic properties of La-BaM hexaferrites by Ni substitution

Hafiz T. Ali[1], M. Ramzan[2], M Imran Arshad[2], Nicola A. Morley[3], M. Hassan Abbas[2], Mohammad Yusuf[4], Atta Ur Rehman[2], Khalid Mahmood[2], Adnan Ali[2], Nasir Amin[2], and M. Ajaz-un-Nabi[2,†]

[1] *Department of Mechanical Engineering, College of Engineering, Taif University, Taif* 21944, *Saudi Arabia*
[2] *Department of Physics, Government College University, Faisalabad, Pakistan*
[3] *Department of Materials Science and Engineering, University of Sheffield, Sir Robert Hadfield Building, Mapping St., Sheffield, S*1 3*JD, UK*
[4] *Department of Clinical Pharmacy, College of Pharmacy, Taif University, Taif* 21944, *Saudi Arabia*

(Received 4 April 2021; revised manuscript received 12 July 2021; accepted manuscript online 14 July 2021)

We investigate the impact of Ni insertion on the structural, optical, and magnetic properties of $Ba_{0.8}La_{0.2}Fe_{12-x}Ni_xO_{19}$ hexaferrites (Ni substituted La-BaM hexaferrites). Samples were prepared using the conventional co-precipitation method and sintered at 1000 °C for 4 hours to assist the crystallization process. An analysis of the structure of the samples was carried out using an x-ray diffraction (XRD) spectrometer. The M-type hexagonal structure of all the samples was confirmed using XRD spectra. The lattice parameters a and c were found to be in the ranges of 5.8925 ± 0.001 nm–5.8952 ± 0.001 nm and 23.2123 ± 0.001 nm–23.2219 ± 0.001 nm, respectively. The M-type hexagonal nature of the prepared samples was also indicated by the presence of corresponding FT-IR bands and Raman modes in the FT-IR and Raman spectra, respectively. EDX results confirmed the successful synthesis of the samples according to the required stoichiometric ratio. A UV-vis spectrometer was used to record the absorption spectra of the prepared samples in the wavelength range of 200 nm–1100 nm. The optical energy bandgap of the samples was found to be in the range of 1.21 eV–3.39 eV. The M–H loops of the samples were measured at room temperature at an applied magnetic field range of 0 kOe–60 kOe. A high saturation magnetization of 99.92 emu/g was recorded in the sample with $x = 0$ at a microwave operating frequency of 22.2 GHz. This high value of saturation magnetization is due to the substitution of La^{3+} ions at the spin-up (12k, 2a, and 2b) sites. The Ni substitution is proven to be a potential candidate for the tuning of the optical and magnetic parameters of M-type hexaferrites. Therefore, we suggest that the prepared samples are suitable for use in magneto-optic applications.

Keywords: M-type hexaferrite, nanostructured materials, magnetic properties, optical properties

PACS: 75.50.–y, 75.75.–c

DOI: 10.1088/1674-1056/ac1412

1. Introduction

In recent years, hexagonal magnetic nanoparticles have attracted great scientific interest due to their potential for use in various technological applications such as permanent magnets, microwave absorbers, highdensity magnetic media, magneto-optic recording media, and stealth technology.[1–4] Hexagonal ferrites are divided into five sub-categories based on their crystal structure and chemical formula: M-type ($AFe_{12}O_{19}$), W-type ($AFe_{16}O_{27}$), X-type ($AFe_{28}O_{46}$), Y-type ($AFe_{12}O_{22}$), and Z-type ($AFe_{24}O_{41}$), where A is the divalent cation such as Ba^{2+}, Sr^{2+}, Pb^{2+}, Ca^{2+}.[5–7] Among these, M-type hexaferrites have gained more attention due to their distinguished properties, such as their very high magnetic anisotropy, higher coercivity, higher corrosion resistance, and high thermal and chemical stability.[8–11] Barium M-type (BaM) hexaferrites are ferrimagnetic materials with the chemical formula $BaFe_{12}O_{19}$ and the space group $P6_3/mmc$. They consist of tetrahedral (4f_1), octahedral (12k, 4f_2, and 2a), and hexahedral (2b) sites. Fe^{3+} ions at the 4f_1 and 4f_2 sites (eight ions per unit cell) exhibit a spin-down character and Fe^{3+} ions at the 12k, 2a, and 2b sites (sixteen ions in a unit cell) exhibit a spin-up character.[12,13] The substitution of various magnetic and non-magnetic ions at these sites can modify the structural, magnetic, and other properties of BaM ferrites. Some examples of substitution at different sites of the hexaferrite structure are divalent ion (A^{2+}) substitution,[14,15] trivalent ion (A^{3+}) substitution,[16,17] and tetravalent ion (A^{4+}) substitution.[14,18] To achieve the best hexaferrite properties, it is very important to optimize the quantity and type of the substituent cations. Various reports have been published on the topic of modifying the microstructure, electrical, dielectric, optical, and magnetic properties of BaM hexaferrite by replacing the Fe^{3+} and Ba^{3+} cations with divalent and trivalent cations. Recently, Cernea *et al.*[9] reported the magnetic properties of Ni^{2+} substituted $BaFe_{12}O_{19}$ hexaferrite. They observed a decreasing trend in the coercivity, retentivity, and maximum energy product with an increase in Ni^{2+}. Iqbal *et al.*[19] studied the effect of Pr–Ni substitution in the crystal lattice of BaSr hexaferrite. They reported an increase in the electrical resistivity of the prepared samples with an increase in the Ni content. Behera *et al.*[20] also investigated the effect of Ni^{2+} incorporation in the lattice matrix of

†Corresponding author. E-mail: majazunnabi@gcuf.edu.pk
© 2022 Chinese Physical Society and IOP Publishing Ltd

$BaFe_{12}O_{19}$ synthesized by the sol–gel method. They found a reduction in the saturation magnetization from 68.16 emu/g to 58.99 emu/g when the Ni^{2+} content (x) increased from 0 to 0.5, and an increase in the ferrimagnetic transition temperature (T_C) was observed. Guner *et al.*[21] reported the synthesis of Bi and La doped BaM hexaferrite by the sol-gel autocombustion method. They studied the dependence of the magnetic properties of $BaFe_{12}O_{19}$ on the concentrations of various dopants such as La, Bi, and Y. They reported the saturation magnetization and coercivity of the prepared samples in the range of 53.69 emu/g–67.42 emu/g and 3.812×10^5 A/m–2.177×10^5 A/m, respectively. Some other reports describe attempts to modify the structural, electrical, optical, or magnetic properties of BaM by doping with Ni^{2+}, La^{3+}, and the co-doping of these cations.[19,22–25] However, a detailed study exploring the impact of Ni^{2+} doping on the structural, optical, and magnetic properties of La-BaM hexaferrites is still needed. High coercivity, moderate saturation magnetization, and low cost are all advantages of these materials. The objective of this work is to provide a detailed study of the impact of Ni^{2+} substitution in La-BaM hexaferrites. A series of samples with the chemical formula $Ba_{0.8}La_{0.2}Fe_{12-x}Ni_xO_{19}$ (Ni-doped BL) hexaferrites was prepared via the co-precipitation route. The co-precipitation method was chosen due to its simplicity, low cost, normal temperature, reduced duration, and the homogeneity of prepared nanoparticles.[26,27] The prepared samples were investigated using different techniques including x-ray diffraction (XRD), energy dispersive x-ray (EDX) spectroscopy, Fourier transform infrared (FTIR) spectroscopy, Raman spectroscopy, UV-vis spectroscopy, and vibrating sample magnetometry (VSM).

2. Experimental details

2.1. Synthesis

In this study, $Ba_{0.8}La_{0.2}Fe_{12-x}Ni_xO_{19}$ ($x = 0, 0.1, 0.2, 0.3, 0.4, 0.5$) ferrites were prepared by the co-precipitation method. The starting materials $BaCl_2{\cdot}2H_2O$, $Ni(NO_3)_2{\cdot}6H_2O$, $Fe(NO_3)_3{\cdot}9H_2O$, and $La(NO_3)_3{\cdot}6H_2O$ were purchased from Aldrich and used as received. The required amounts of these chemicals were used to prepare a homogeneous solution in deionized water according to the required stoichiometric ratios. The solution was stirred magnetically on a hotplate at a temperature 70 °C until the formation of precipitates occurred. The pH of the solution was maintained at 11 during the precipitation process by adding NaOH dropwise. The samples were placed in a water bath for 12 hours at 90 °C to complete the digestion process. The precipitates were laid down at the bottom of the beakers. These precipitates were collected and cleaned with DI water and ethanol to remove impurities. The drying of the washed precipitates was accomplished by placing them in the oven for 15 hours at 110 °C. The dried precipitates were then ground using a mortar and pestle to obtain fine powder samples. The samples were sintered at 1000 °C in a muffle furnace for four hours to assist the crystallization process. The cooling was done at a very slow rate ($\sim$ 1.4 °C) to avoid the development of pores.

2.2. Characterization

A phase and microstructure analysis of the sintered samples was carried out using an x-ray diffractometer (D8 Advance, Bruker), with Cu $K\alpha$ as the x-ray source. The diffraction patterns were recorded in the 2θ range of 20°–60°. An FT-IR spectrometer (Spectrum 2, PerkinElmer) was used to obtain the infrared spectra. An EDX spectrometer was used to determine the elemental composition of the prepared samples. The Raman spectra were recorded in the wavenumber range of 150 cm^{-1}–800 cm^{-1} using a Raman spectrometer. The optical energy bandgap values were determined using a UV-Vis spectrometer (double beam, Lambda 25, PerkinElmer). The magnetic character of the sintered samples was studied by recording M–H loops at room temperature using a vibrating sample magnetometer (Lakeshore-7407).

3. Results and discussion

3.1. Phase analysis

The XRD spectra of the synthesized Ni-doped La-BaM hexaferrites, as shown in Fig. 1, were recorded at 300 K. A comparison of the XRD patterns revealed that all the labeled peaks were well-matched with the JCPDS data (card #00-051-1879) for BaM hexaferrites, and that no extra peaks were observed. This confirms the formation of a single-phase magneto-plumbite structure with the space group $P6_3/mmc$ to a very high accuracy and without any defects or impurity phase. The various crystal structure parameters including the lattice constants (a & c),[28] crystallite size, unit cell volume,[8] x-ray density,[26] and dislocation density[29,30] are calculated utilizing the indexed XRD patterns; the calculated parameters are presented in Table 1. From Fig. 2, it can be observed that the lattice constant a increased with an increased Ni^{2+} ion content, and c also increased with the addition of doping except at $x = 0.3$. It can also be seen in Fig. 2 that the unit cell volume (V) was enhanced by the substitution of dopant ions. This increase is attributed to the difference in the ionic radii of Ni^{2+} (0.69 Å) and Fe^{3+} (0.64 Å).[20] The average crystallite size of the prepared nanoparticles was found to be in the range of 25.2 ± 0.1 nm–28.5 ± 0.1 nm and showed a decreasing trend with an increase in the Ni^{2+} ion concentration. The calculated x-ray density of the samples was found to lie in the range of 5.144 g/cm^3–5.310 g/cm^3. The dislocation density of a material is inversely proportional to the square of the crystallite size and provides information about the strength of the material.[29,30] The calculated values of the dislocation density of the prepared nanoparticles revealed that the sample with $x = 0.1$ had the minimum value of dislocation density.

Table 1. Concentrations of Ni^{2+} and calculated structural parameters of $Ba_{0.8}La_{0.2}Fe_{12-x}Ni_xO_{19}$ hexaferrites.

Parameters	$x=0$	$x=0.1$	$x=0.2$	$x=0.3$	$x=0.4$	$x=0.5$
Lattice parameter a (Å) ± 0.001	5.8925	5.8934	5.8937	5.8943	5.8951	5.8952
Lattice parameter c (Å) ± 0.001	23.2123	23.2189	23.2201	23.2191	23.2219	23.2218
Unit cell volume V (Å) ± 0.006	697.96	698.37	698.48	698.59	698.87	698.89
Crystallite size D (nm) ± 0.1	27.9	28.5	27.8	26.6	26.2	25.2
X-ray density D_X (g/cm^3)	5.310	5.299	5.304	5.144	5.229	5.219
Dislocation density ρ (10^{11} cm^{-2})	1.280	1.227	1.291	1.413	1.460	1.579

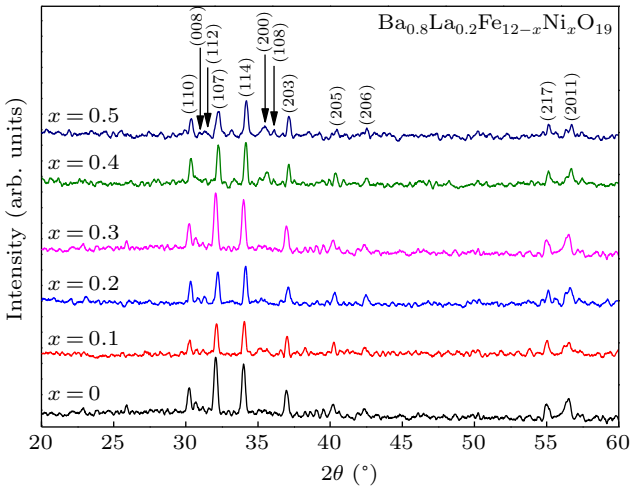


Fig. 1. XRD patterns of the synthesized $Ba_{0.8}La_{0.2}Fe_{12-x}Ni_xO_{19}$ hexaferrite powders.

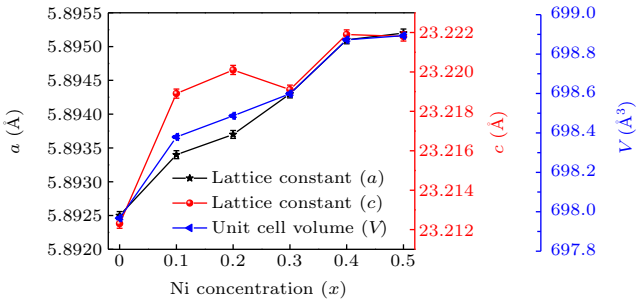


Fig. 2. Plot of the lattice parameters (a & c) and unit cell volume (V) as a function of the Ni^{2+} content in the synthesized hexaferrite samples.

3.2. Elemental composition analysis

The elemental composition of the synthesized samples was analyzed quantitatively using EDX spectroscopy; the results are presented in Table 2. The observed composition of all the elements was a good match for the expected stoichiometric composition. The results confirmed that La^{3+} and Ni^{2+} cations had been substituted for Ba and Fe cations at the appropriate ratios.

Table 2. Elemental composition of $Ba_{0.8}La_{0.2}Fe_{12-x}Ni_xO_{19}$ M-type hexaferrites obtained by EDX.

Samples	Elemental composition (%)				
	Ba	La	Ni	Fe	O
$Ba_{0.8}La_{0.2}Fe_{12}O_{19}$	2.52	0.64	0.00	37.29	59.55
$Ba_{0.8}La_{0.2}Fe_{11.9}Ni_{0.1}O_{19}$	2.51	0.65	0.31	36.92	59.61
$Ba_{0.8}La_{0.2}Fe_{11.8}Ni_{0.2}O_{19}$	2.60	0.61	0.63	37.16	59.00
$Ba_{0.8}La_{0.2}Fe_{11.7}Ni_{0.3}O_{19}$	2.56	0.63	0.94	36.22	59.65
$Ba_{0.8}La_{0.2}Fe_{11.6}Ni_{0.4}O_{19}$	2.49	0.64	1.27	35.72	59.88
$Ba_{0.8}La_{0.2}Fe_{11.5}Ni_{0.5}O_{19}$	2.69	0.64	1.54	35.69	59.44

3.3. Functional group analysis

The FTIR spectra of the prepared powder were recorded in the range of 4000 cm^{-1}–400 cm^{-1} and are presented in Fig. 3. The absorption bands around 430 cm^{-1} and 580 cm^{-1} are the two featured bands of M-type hexaferrites, which were observed in all the samples, with minor variations in the positions and relative intensities. The band observed at around 430 cm^{-1} relates to the octahedral Fe–O bond, while the band at around 580 cm^{-1} is due to the stretching vibrations of the tetrahedral Ba–O bond.[31,32] The presence of these bonds confirmed the formation of the BaM hexagonal structure. The doublet peak at 2361 cm^{-1} originates from ambient CO_2 gas.

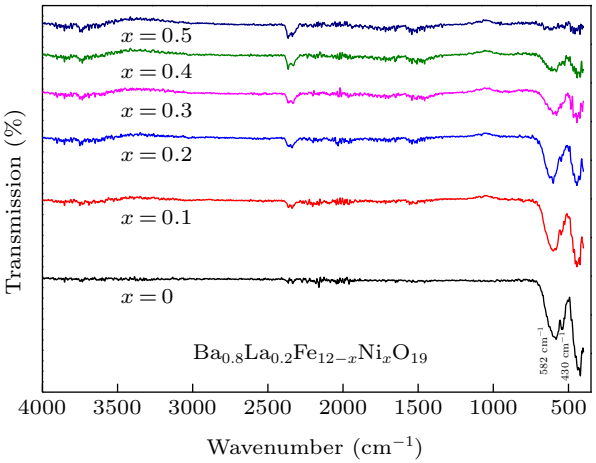


Fig. 3. FTIR spectra of the synthesized hexaferrite samples.

3.4. Raman analysis

The Raman spectra of the hexaferrite samples are shown in Fig. 4. According to group theory, 42 active Raman modes $\Gamma_{\text{Raman}} = 11A_{1g} + 14E_{1g} + 17E_{2g}$ arise due to the vibrations of 64 atoms at various sites in the unit cell.[33] In our samples, active Raman modes are observed at around 284.71, 335.22, 410.28, 457.21, 522.13, 613.52, and 684.87 cm^{-1}, which confirms the formation of the BaM phase. The peaks present at around 684.87 cm^{-1} are due to the A_{1g} vibration of Fe–O bonds at the octahedral $4f_1$ site and the bipyramidal $2b$ site. Furthermore, the peaks at 457.21 cm^{-1} are also due to the A_{1g} vibration of Fe–O bonds at the octahedral 2a site. The peaks at around 613.52 cm^{-1} and 410.28 cm^{-1} are attributed

to the A_{1g} vibration of Fe–O bonds at the octahedral $4f_2$ and $12k$ sites respectively. The Raman modes observed at around 522.13 cm^{-1} and 284.71 cm^{-1} are attributed to E_{1g} vibration. Moreover, the peaks at 335.22 cm^{-1} are attributed to E_{2g} vibrations. The small variations found in the peak positions are attributed to the substitution of Ni^{2+} ions in the BaM lattice.[31,34–36]

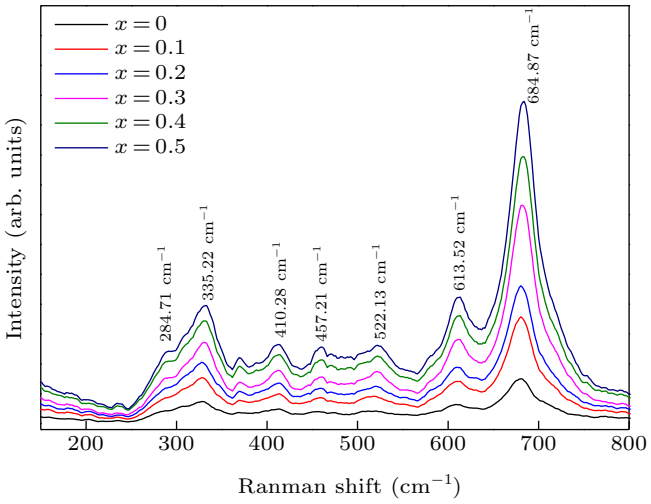


Fig. 4. Raman spectra of the Ni^{2+} substituted Ba-La hexaferrite samples.

3.5. UV-vis analysis

The absorption spectra and optical energy bandgap are related, as given by Tauc's relation: $\alpha(h\nu) = A(h\nu - E_g)^n$,[37–39] where A and α represent a constant and the absorption coefficient, respectively, and n takes values of 1/2 for direct and 2 for indirect transitions. Tauc plots of the prepared samples are presented in Fig. 5. The obtained values of the optical energy bandgaps lie in the range of 1.21 eV–3.39 eV and are plotted as a function of the Ni^{2+} ion content, as shown in Fig. 6. It can be seen from Fig. 6 that the optical bandgap is

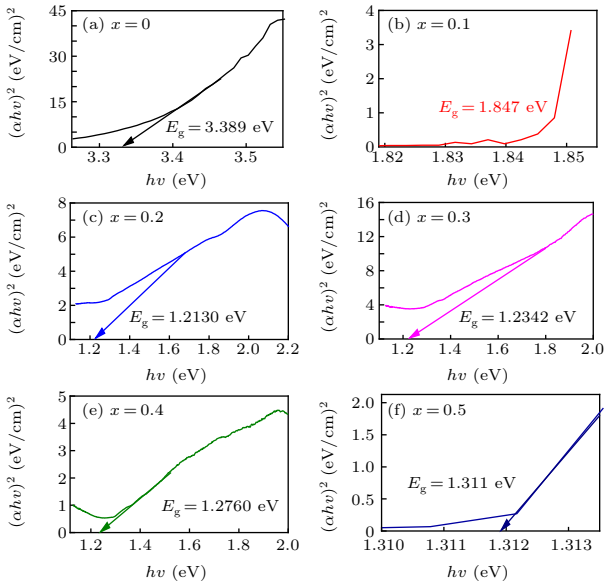


Fig. 5. Plot of $(\alpha h\nu)^2$ versus the photon energy $(h\nu)$ for the prepared hexaferrite nanoparticles.

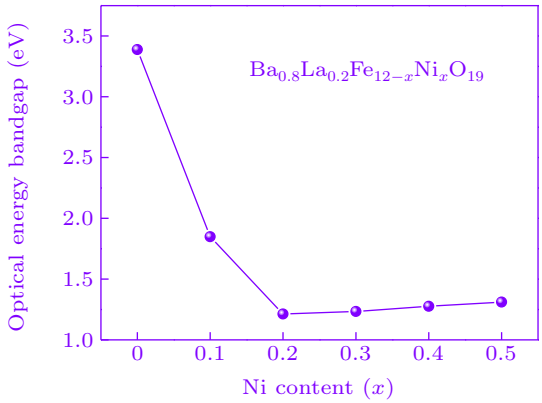


Fig. 6. Plot of the energy bandgap as a function of the Ni^{2+} ion content.

drastically decreased by the incorporation of a small amount of Ni^{2+} at values of x up to $x = 0.2$, however, a further increase in the Ni^{2+} concentration does not have a significant effect on the bandgap values.[26,31,40–44] These results suggest that the synthesized samples are potential candidates for use in various optoelectronic applications.

3.6. Magnetic hysteresis loop analysis

The magnetic hysteresis (M–H) loops of the synthesized nanohexaferrite samples were recorded at 300 K and are depicted in Fig. 7. The M–H loops of all the samples show a hard magnetic nature. Various magnetic parameters, including the saturation magnetization (M_s), magnetic retentivity (M_r), coercivity (H_c), and squareness ratio (M_r/M_s) are measured from the M–H loops and are given in Table 3. The maximum observed value of saturation magnetization is 99.92 emu/g for the sample with $x = 0$, which reduced to 40.8 emu/g for the sample with $x = 0.5$. According to previous research, Fe^{3+} ions exhibit various magnetic moments at different sites. As a result, the preferred sites of magnetic Ni^{2+} ions determine the material's overall magnetization. The Ni^{2+} has a magnetic nature, but a low magnetic moment compared to Fe^{3+}. It was reported previously that Ni^{2+} ions prefer to substitute for Fe^{3+} ions at $4f_2$ and $12k$ at low concentrations and at the $12k$ sites for higher concentrations. The substitution of Ni^{2+} ($2\mu_B$) ions at the Fe^{3+} ($5\mu_B$) ion sites is responsible for the decrease in saturation magnetization with increasing Ni^{2+} concentration.[15,20,31,45] The saturation magnetization values that are achieved in this study for Ni^{2+} free samples are compared with the values reported in the literature[4,9,20,45–47] and are found to be significantly higher. The higher values of saturation magnetization achieved are attributed to the vacancy free nature of the samples and the presence of paramagnetic La^{3+} cations at the spin-up ($12k$, $2a$, and $2b$) sites.[48,49] The magnetic retentivity M_r, coercivity H_c, and squareness ratio (M_r/M_s) also decreased with an increase in the Ni^{2+} content. A graphical representation of the Ni^{2+} contents versus the saturation magnetization (M_s) and the magnetic retentivity (M_r) are shown in Fig. 8. Magneto-crystalline anisotropy

is known to be responsible for the variations in the magnetic retentivity, coercivity, and squareness ratio values of ferrite materials.[20] The microwave frequency (ω_m) is determined using the relation $\omega_m = 8\pi^2 M_s \gamma$, where γ is a gyromagnetic fraction with the significance of 2.8 MHz/Oe, and M_s is the saturation magnetization.[50] The applied field versus the microwave operating frequency (ω_m) of the prepared hexaferrites samples is plotted in Fig. 9. It can be seen in Fig. 9 that the range of microwave operating frequencies (ω_m) is 8.80 GHz–22.2 GHz, indicating that the prepared hexaferrites are applicable in longitudinal recording media, data storage magnetic devices, and microwave absorption.

Table 3. Magnetic parameters of the prepared hexaferrites.

Samples	M_s (emu/g)	M_r (emu/g)	H_c (Oe)	M_r/M_s	ω_m (GHz)
$Ba_{0.8}La_{0.2}Fe_{12}O_{19}$	99.92	40.3	5132.9	0.40332	22.2
$Ba_{0.8}La_{0.2}Fe_{11.9}Ni_{0.1}O_{19}$	86.2	34.8	5037.7	0.40371	19.2
$Ba_{0.8}La_{0.2}Fe_{11.8}Ni_{0.2}O_{19}$	77.1	24.4	3336.3	0.31647	17.1
$Ba_{0.8}La_{0.2}Fe_{11.7}Ni_{0.3}O_{19}$	70.3	27.2	3217.2	0.38691	15.7
$Ba_{0.8}La_{0.2}Fe_{11.6}Ni_{0.4}O_{19}$	56.5	13.7	1154.9	0.24248	12.6
$Ba_{0.8}La_{0.2}Fe_{11.5}Ni_{0.5}O_{19}$	40.8	18.6	2034.8	0.45588	8.8

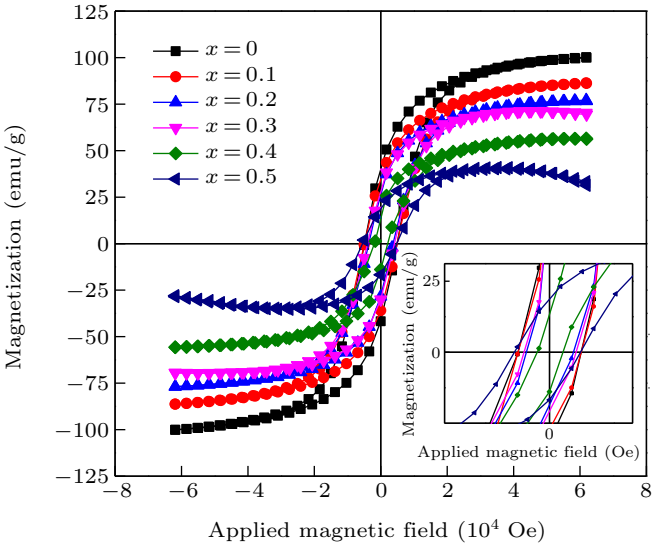


Fig. 7. The M–H loops for the Ni^{2+} doped Ba–La hexaferrites.

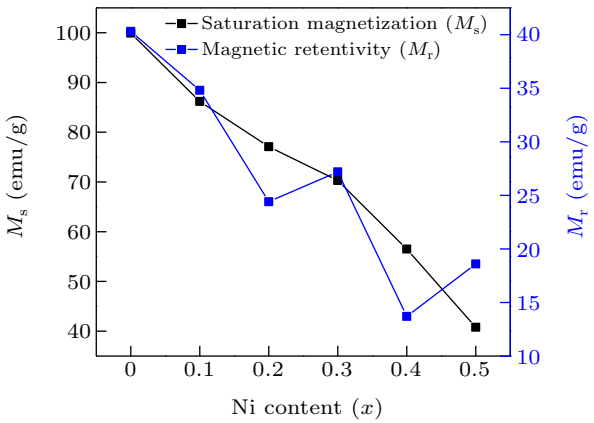


Fig. 8. Plot of the saturation magnetization and remanent magnetization of the synthesized samples as a function of the Ni content.

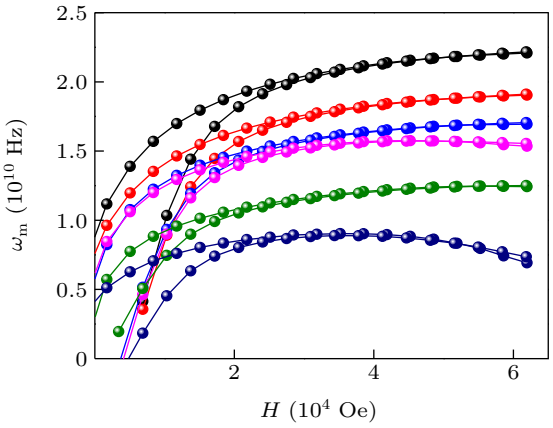


Fig. 9. Applied field versus microwave operating frequency.

4. Conclusion

The BaM nanoferrites with the general formula $Ba_{0.8}La_{0.2}Fe_{12-x}Ni_xO_{19}$ ($0 \le x \le 0.5$) were synthesized by the co-precipitation route. The prepared powders were densified using conventional sintering processing at 1000 °C for 4 h. A phase confirmation and a structural analysis were carried out using XRD and the average crystallite size of the samples was found to be in the range of 25.2 ± 0.1 nm–28.5 ± 0.1 nm. The optical properties of the prepared samples were investigated using UV-vis spectroscopy and it was found that the optical energy bandgap lies in the range 1.21 eV–3.39 eV. A high value of saturation magnetization M_s (99.92 emu/g) was achieved for the sample with $x = 0$, which makes La-BaM hexaferrites suitable for operation in the significantly higher frequency range of up to 22.2 GHz. The magnetic parameters (M_s, M_r, H_c, and M_r/M_s) of the prepared samples show a decreasing trend with an increase in the Ni content. The optical and magnetic properties of the Ni^{2+} substituted BaM hexaferrites suggest that these samples are potential candidates for use in magnetic storage, microwave frequency absorption devices, and magneto-optical devices.

Acknowledgment

Project supported by the Taif University Researchers Supporting Project number (TURSP-2020/293), Taif University, Taif, Saudi Arabia.

References

[1] Jayakumar T, Raja C R and Arumugam S 2020 *J. Mater. Sci. Mater. Electron.* **31** 16308
[2] Akbarzadeh A, Samiei M and Davaran S 2012 *Nanoscale Res. Lett.* **7** 1
[3] Waqar M, Rafiq M A, Mirza T A, Khalid F A, Khaliq A, Anwar M S and Saleem M 2018 *Appl. Phys. A* **124** 1
[4] Ramzan M, Arshad M I, Sharif M, Mahmood K, Ali A, Amin N and Ajaz-un-Nabi M 2019 *J. Supercond. Nov. Magn.* **32** 3517
[5] Almessiere M A, Slimani Y, El Sayed H S and Baykal A 2018 *J. Sol-Gel Sci. Technol.* **88** 628
[6] Singhal S, Garg A N and Chandra K 2005 *J. Magn. Magn. Mater.* **285** 193

[7] Pullar R C 2012 *Prog. Mater. Sci.* **57** 1191
[8] Yasmin N, Yasmin S, Zahid M, Gillani S F, Islam M U, Altaf M and Mirza M 2020 *Physica B* **581** 411950
[9] Cernea M, Greculeasa S G, Radu R, Aldica G, Ganea P, Surdu V A and Costescu R M 2020 *J. Alloys Compd.* **831** 154850
[10] Mitra C, Ram S and Venimadhav A 2012 *J. Alloys Compd.* **545** 225
[11] Li Y, Wang Q and Yang H 2009 *Curr. Appl. Phys.* **9** 1375
[12] Özgür Ü, Alivov Y and Morkoç H 2009 *J. Mater. Sci. Mater. Electron.* **20** 789
[13] Janasi S R, Rodrigues D, Landgraf F J and Emura M 2000 *IEEE Transactions on Magnetics* **36** 3327
[14] Beevers J E, Love C J, Lazarov V K, Cavill S A, Izadkhah H, Vittoria C and Dhesi S S 2018 *Appl. Phys. Lett.* **112** 082401
[15] Baykal A, Auwal I A, Güner S and Sözeri H 2017 *J. Magn. Magn. Mater.* **430** 29
[16] Ramzan M, Arshad M, Amin N, Mahmood K, ALIa A, Sharif M and Ajaz-Un-Nabi M 2019 *Dig. J. Nanomater. Bios.* **14** 849
[17] Ounnunkad S 2006 *Solid State Commun.* **138** 472
[18] Ashiq M N, Ehsan M F, Iqbal M J and Najam-ul-Haq M 2013 *J. Magn. Magn. Mater.* **332** 93
[19] Iqbal M J and Farooq S 2010 *J. Alloys Compd.* **505** 560
[20] Behera P and Ravi S 2019 *Solid State Sci.* **89** 139
[21] Güner S, Auwal I A, Baykal A and Sözeri H 2016 *J. Magn. Magn. Mater.* **416** 261
[22] Sözeri H, Küçük İ L K E R and Özkan H 2011 *J. Magn. Magn. Mater.* **323** 1799
[23] Li C J, Wang B and Wang J N 2012 *J. Magn. Magn. Mater.* **324** 1305
[24] Vinnik D A, Zherebtsov D A, Mashkovtseva L S, Nemrava S, Semisalova A S, Galimov D M and Niewa R 2015 *J. Alloys Compd.* **628** 480
[25] Tang X, Yang Y and Hu K 2009 *J. Alloys Compd.* **477** 488
[26] Ashraf G A, Zhang L, Abbas W and Murtaza G 2019 *Curr. Appl. Phys.* **19** 506
[27] Jamalian M, Ghasemi A and Asl M J P 2015 *J. Electron. Mater.* **44** 2856
[28] Cullity B D 1978 *Plane Spacings In Lattice Geometry In Elements of X-Ray Diffraction* (Addison-Wesley publishing company Inc.)
[29] El-Sayed S M, Meaz T M, Amer M A and El Shersaby H A 2014 *Particul. Sci. Technol.* **32** 39
[30] Amjad T, Sadiq I, Javaid A B, Riaz S, Naseem S and Nadeem M 2019 *J. Alloys Compd.* **770** 1112
[31] Auwal I A, Baykal A, Guner S, Sertkol M and Sozeri H 2016 *J. Magn. Magn. Mater.* **409** 92
[32] Kaur T, Kumar S, Bhat B H, Want B and Srivastava A K 2015 *Appl. Phys. A* **119** 1531
[33] Kreisel J, Lucazeau G and Vincent H 1998 *J. Solid-State Chem.* **137** 127
[34] Wu C, Yu Z, Yang Y, Sun K, Nie J, Liu Y and Lan Z 2016 *J. Alloys Compd.* **664** 406
[35] Buzinaro M A P, Ferreira N S, Cunha F and Macêdo M A 2016 *Ceram. Int.* **42** 5865
[36] Morel A, Le Breton J M, Kreisel J, Wiesinger G, Kools F and Tenaud P 2002 *J. Magn. Magn. Mater.* **242–245** 1405
[37] Ashraf G A, Zhang L, Abbas W and Murtaza G 2018 *Ceram. Int.* **44** 18678
[38] Aslam A, Razzaq A, Naz S, Amin N, Arshad M I, Nabi M A U and Ur Rehman A 2021 *J. Supercond. Nov. Magn.* **34** 1855
[39] Aslam A, Rehman A U, Amin N, un Nabi M A, ul ain Abdullah Q, Morley N A and Mehmood K 2021 *J. Phys. Chem. Solids* **154** 110080
[40] Karmakar M, Mondal B, Pal M and Mukherjee K 2014 *Sensor. Actuat. B: Chem.* **190** 627
[41] Valero-Luna C, Palomares-Sanchéz S A and Ruíz F 2016 *Catal. Today* **266** 110
[42] Hussain K, Amin N and Arshad M I 2021 *Ceram. Int.* **47** 3401
[43] ALIa I, Amin N, Rehman A, Akhtar M, Fatima M, Mahmood K and Arshad M I 2020 *Dig. J. Nanomater. Bios.* **15** 1
[44] Amin N, Akhtar M, Sabir M, Mahmood K, ALIa A, Mustafa G and Arshad M 2020 *J. Ovonic Res.* **16** 11
[45] Alsmadi A M, Bsoul I, Mahmood S H, Alnawashi G, Prokeš K, Siemensmeyer K and Nakotte H 2013 *J. Appl. Phys.* **114** 243910
[46] Kamzin A S, Rozenbaum V L and Ol'khovik L P 1999 *Phys. Solid State* **41** 433
[47] Afghahi S S S, Jafarian M, Salehi M and Atassi Y 2017 *J. Magn. Magn. Mater.* **421** 340
[48] Liu X, Zhong W, Yang S, Yu Z, Gu B and Du Y 2002 *J. Magn. Magn. Mater.* **238** 207
[49] Liu X, Hernandez-Gomez P, Huang K, Zhou S, Wang Y, Cai X and Ma B 2006 *J. Magn. Magn. Mater.* **305** 524
[50] Rehman A U, Morley N A, Amin N, Arshad M I, un–Nabi M A, Mahmood K and Alzaid M 2020 2020 *Ceram. Int.* **46** 29297